Received: 15 September 2025 | Revised: 26 June 2026 | Accepted: 14 July 2026

DOI: 10.1002/qj.70280

Quarterly Journal of the Royal Meteorological Society RMetS

RESEARCH ARTICLE

Stratospheric influence on tropical cyclone evolution

Andrea Davin[1] | **Giousef Alexandros Charinti[2]** | **Caroline Muller[2]** | **Andrea Polesello[2]** | **Claudia Pasquero[1]**

[1]Department of Earth and Environmental Sciences, University of Milan–Bicocca, Milan, Italy

[2]Institute of Science and Technology Austria, Klosterneuburg, Austria

Correspondence
Andrea Davin, Department of Earth and Environmental Sciences, University of Milan–Bicocca, Milan, Italy.
Email: a.davin@campus.unimib.it

Funding information
National Recovery and Resilience Plan project TeRABIT, Grant/Award Numbers: IR0000022, PNRRMissione4, Componente2, Investimento3.1, CUPI53C21000370006; H2020 European Research Council, Grant/Award Number: 805041

Abstract

Physical processes at play in the genesis and evolution of tropical cyclones are conducive to the formation of warm cores at their centres. When the warm anomaly is particularly large in the upper troposphere, it is referred to as a high-level warm core. Previous works documented the generation of high-level warm cores as a consequence of stratospheric air intrusion into the troposphere induced by the upper-level dynamics of a tropical cyclone. However, little attention has been given to their effects on the storm's subsequent evolution. It has been suggested that the presence of a high-level warm core can have opposite effects on tropical cyclone intensity: both strengthening and weakening have been described as possible consequences of its formation. In this study, we examine the role of high-level warm cores in the intensification and dissipation processes of tropical cyclones, as reproduced in numerical models of different complexities, namely the model "System for Atmospheric Modeling" (SAM) run under idealized conditions and the model Nonhydrostatic ICosahedral Atmospheric Model run under realistic conditions following the DYnamics of the Atmospheric general circulation Modeled On Non-hydrostatic Domains summer protocol. Our results confirm the hypothesis of a stratospheric origin behind the formation of high-level warm cores. Their initial role is shown to be an enhancement of storm intensity, by a lowering of the hydrostatic sea-level pressure (HSLP) associated with the presence of warm air aloft. However, as the warm anomaly intensifies and extends to lower levels, it also increases static stability in the air column, with the consequence of inhibiting convection and ultimately contributing to cyclone dissipation. These findings suggest that high-level warm cores play a dual role in the tropical cyclone life cycle, providing a stabilizing mechanism that can limit cyclone strength and longevity.

KEYWORDS

atmospheric stability, intensification, moist static energy, numerical modelling, stratosphere, tropical cyclones, troposphere

1 INTRODUCTION

Despite significant improvements over the last decades, forecasts of tropical cyclone (TC) intensity still pose important challenges (Cangialosi *et al.*, 2020). The intensification rate (IR) can undergo large changes during a cyclone's lifetime in response to variations in many environmental factors, including vertical shear of horizontal wind and sea-surface temperature inhomogeneities (Kaplan & DeMaria, 2003; Xu & Wang, 2018). Even in the absence of environmental disturbances, the evolution of TC strength is affected by internal dynamical processes such as eyewall replacement cycles (Kossin & Sitkowski, 2012), interactions between vortex asymmetries and updrafts (Kuo *et al.*, 2016), and interplay between inertial and static stability (Schubert & Hack, 1982).

A widely studied mechanism in TC intensification is wind-induced surface heat exchange (WISHE) feedback, which suggests that storm intensification is the result of a positive feedback between surface heat fluxes and wind speed near the cyclone's core (Emanuel, 2003). Under WISHE theory, a mature cyclone can be approximated as a Carnot heat engine fuelled by energy input into the atmosphere at the air–sea interface. Based on these premises, and on the assumption that the troposphere has an adiabatic temperature profile, the theoretical maximum potential intensity (PI) can be derived from the environmental conditions, such as ocean surface and atmospheric boundary-layer enthalpy, along with sea-surface temperature (SST) and upper tropospheric outflow temperature (Bister & Emanuel, 1998, 2002; Emanuel, 1997; Rousseau-Rizzi & Emanuel, 2019). Observations indicate that many cyclones do not reach the theoretical PI (Chacko, 2023; Emanuel, 2000; Lavender *et al.*, 2018; Mei *et al.*, 2012), either because the cyclone along its track encounters unfavourable conditions (strong vertical wind shear, passage over cold water, landfall) or because of self-limiting processes.

Models have been used extensively to study TC evolution in simplified settings, where some of the sources of variation in the IR could be eliminated or controlled. Idealized axisymmetric models of TCs show an evolution composed of an intensification phase up to the PI, which is then maintained nearly constant for a long time (Emanuel, 1995; Rotunno & Emanuel, 1987). The inclusion of the effects of strong winds on SST (cooling by upper-ocean mixing and upwelling) reduces heat fluxes from the ocean, limiting the energy available for the storm. Despite that, the evolution still shows a monotonic intensification up to a reduced peak intensity (Lin *et al.*, 2013; Schade & Emanuel, 1999).

However, other studies indicate a different behaviour. Early works of TC evolution under stationary boundary conditions demonstrated that internal dynamics limiting convective activity lead to a non-monotonic intensity variation (Ooyama, 1969). More recently, high-resolution simulations in idealized radiative convective equilibrium conditions indicate that TC intensity, even in stationary settings, may neither increase steadily toward a theoretical maximum nor reach the theoretical upper limit. Instead, intensity oscillations have been observed (Muller & Romps, 2018; Polesello *et al.*, 2025; Smith *et al.*, 2021; Wing *et al.*, 2016), correlated with variations in convective available potential energy (CAPE) within the storm. This corroborates the interpretation that atmospheric stability can play a key role in shaping cyclone evolution (Polesello *et al.*, 2025). It should be noted that environmental CAPE is not relevant for PI derivation (Bister & Emanuel, 2002; Garner, 2015), which considers uprising air motion in the eyewall driven mainly by frictional convergence, rather than buoyancy. This corresponds to assuming the troposphere to be neutral to moist convection. However, TC-related processes can act to stabilize the air column, limiting the eyewall ascent and breaking the assumptions under which PI theory is formulated.

A driver for air-column stabilization is the formation of a high-level warm core (HWC) in the upper troposphere. The formation of a warm anomaly over the cyclone is favoured by the increasing inertial stability in intensifying storms, which confine warming within the upper layers of the inner-core region (Schubert & Hack, 1982). This, however, might have opposing effects. On the one hand, warmer air aloft increases static stability, which might inhibit deep convection and lead to a weakening of the cyclone (Ooyama, 1969; Rodgers *et al.*, 1990; Wang & Wang, 2014). On the other hand, it reduces hydrostatic sea-level pressure (HSLP: Wang & Wang, 2014) and leads to an increase of the efficiency with which thermodynamic forcing contributes to vortex spin-up (Schubert & Hack, 1982). Indeed, Chen and Zhang (2013) showed that in Hurricane *Wilma* (2005) there was an initial phase of vigorous deep convection associated with weak inertial stability that allowed warming to be advected away from the storm core, limiting intensification. As inertial stability later increased, warming became progressively more confined within the inner core, favouring rapid intensification even as convective burst activity decreased due to enhanced static stability.

The HWC in Hurricane *Wilma* was investigated further by Zhang and Chen (2012). It was shown, using a high-resolution, cloud-permitting numerical simulation produced with the Weather Research and Forecasting (WRF) model, that the generation of the HWC was associated with descending air of stratospheric origin. According to their work, the onset of strong convective bursts (CBs) within the eyewall is what produced subsidence from the stratosphere. In addition, they pointed out that this downward motion coincided with the onset of rapid intensification.

The role of stratospheric air entrainment in HWC formation and TC evolution has been investigated in several works over the last decade. Rodgers *et al.* (1990) analysed the total ozone distribution, which can be considered a tracer of stratospheric air, in TCs formed in the western Atlantic. In their work, they concluded that the observed patterns could be linked to a process of tropopause folding, which leaves room for stratospheric air intrusion in the eye. This intrusion was observed to be more pronounced in intensifying cyclones but, at the same time, the case study of cyclone *Irene* (1981) showed that intrusion of stratospheric air in the eye was associated with reduced inner core convection and later weakening of the cyclone.

The analysis by Ohno and Satoh (2015) of the potential temperature budget equation for the inner-core region added further insight on the formation of HWCs. Their modelling study showed that, thanks to processes such as CBs, in intense cyclones the angular momentum is transported from the troposphere to the lower stratosphere, thus increasing the inertial stability in a region with strong static stability. The increased inertial stability confines the circulation response to diabatic heating in clouds laterally, as horizontal displacements are inhibited (Schubert & Hack, 1982). Therefore, the vertically oriented aspect ratio of the streamfunction leads to substantial downward motion from the lower stratosphere, which leads to the formation of HWCs. The novelty of their findings was that previously the upper-level warming was related solely to CBs, which are generally markers of the early stages of TCs, while their study described a mechanism that explains the formation of upper-level warming even in the mature stages of TCs. In any case, the two mechanisms are not mutually exclusive.

Kieu *et al.* (2016) developed a mathematical model to understand the mechanisms behind HWC formation. In their work, they proposed two different mechanisms for the formation of a HWC. The first may activate when a TC is intense enough to pierce through the tropopause: in this scenario, the TC forms clouds in the low stratosphere surrounding the eye. The radiative cooling of the clouds forms a cold annulus, which generates an inward pressure gradient in the 100–70 hPa layer that forces stratospheric air subsidence in the eye. The second mechanism involves the formation of an inner warm annulus originated by the returning inflow associated with overshooting convective rings in the eyewall region. They verified the validity of their model by numerical analysis of a cyclone produced using the model Hurricane-WRF (HWRF), which showed that in either case the vertical advection of potential temperature from the stratosphere is what contributes most to the formation of HWCs.

More recently, Moon and Kieu (2017) showed that the prominence of HWCs and their influence on TC intensity are modulated by tropopause height and lower stratospheric stratification. Running sensitivity tests on HWRF, they showed that the intensity of TCs at their mature stage is inversely correlated to prestorm tropopause height. Also, they showed how a weaker stratification of the lower stratosphere leads to warmer HWCs and more intense cyclones. These results support the idea that HWCs develop from subsidence of stratospheric air, favoured by a relatively weak static stability in the stratosphere.

The previously mentioned works mention several mechanisms associated with the HWC that can affect the intensity of the cyclone, such as modification of the upper-level divergence via a strengthening of the outflow jet or the advection of potential vorticity into the upper inner region of the cyclone (Ohno & Satoh, 2015; Rodgers *et al.*, 1990). Mostly, however, they focus on how the formation of a HWC can be inductive of TC intensification by reducing the HSLP in the eye and increasing the efficiency of the conversion from thermal to kinetic energy (Kieu *et al.*, 2016; Moon & Kieu, 2017; Schubert & Hack, 1982; Zhang & Chen, 2012). In this work, we quantify this effect and delve further into its stabilizing effect on the air column. Although the TC weakening induced by an increased stability was cited in a few previous works (Ohno & Satoh, 2015; Ooyama, 1969; Polesello *et al.*, 2025), we aim to gain a better understanding of the regulatory effect that HWCs have on TC evolution. By analysing numerical simulations of models with different complexities and realism levels, this study focuses on the identification of the mechanisms by which stratospheric air intrusions and HWCs modulate cyclone intensity.

2 | METHODS

We investigate the evolution of TCs and the development of HWCs in high-resolution numerical simulations, first in an idealized setting and then under more realistic conditions. In this section, we describe the two simulation setups, followed by a discussion of the analyses performed on their outputs. Figure 1 introduces some of the differences between the two setups in terms of resolution, spatial domain, and configuration, with the realistic simulation including a land–sea mask.

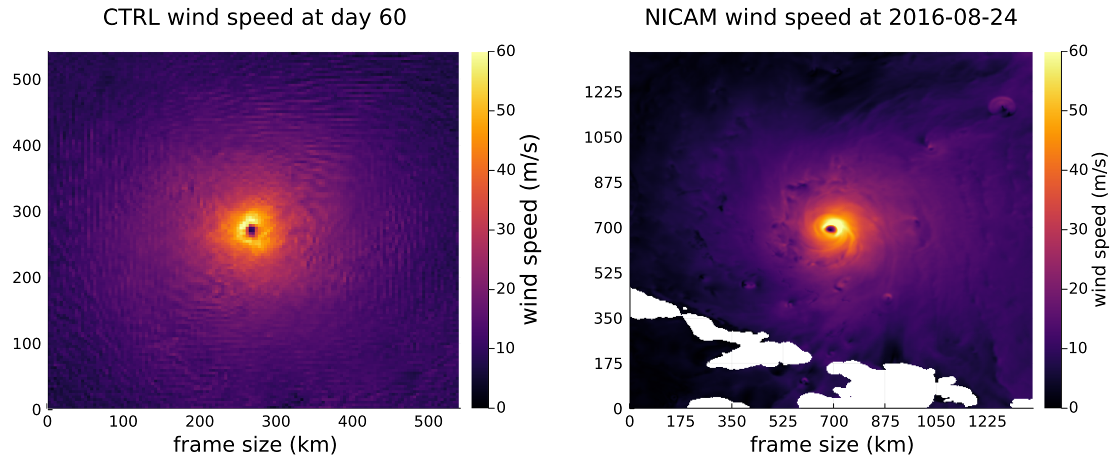

FIGURE 1 Snapshot of near-surface wind speed for CTRL (z = 37.5 m, left) and NICAM (z = 33.16 m, right) cyclones during their intensification phase. In the right panel, the cyclone is centred at 25.1°N, −73.8°E, and the model land mask (white shading) represents the Bahamas islands. Note the two different domain sizes.

2.1 | Tropical cyclone in an idealized setting

We employ the cloud-resolving model (CRM) "System for Atmospheric Modeling" (SAM) version 6.11.1 (Khairoutdinov & Randall, 2003). This model solves the anelastic equations of conservation for momentum, mass, energy, and water, on a high-resolution spatial grid (4-km horizontal grid spacing and 53 unevenly spaced vertical levels starting at 38.5 m and reaching about 18 km). We run the model in the idealized setting of radiative–convective equilibrium, on a doubly periodic square domain with sides of 1024 km, set in an ocean-only environment with fixed SST. The setup for this simulation is detailed further in Polesello *et al.* (2025), where readers can find additional context. Briefly, the SST is fixed at 300 K and the Coriolis parameter is set to $f = 10^{-4}\ \mathrm{s}^{-1}$, which was raised from the typical value of the tropical regions ($\simeq 5 \times 10^{-5}\ \mathrm{s}^{-1}$) to reduce the size of the cyclone and limit the computational effort needed to simulate it. Interactive radiation was used, but the diurnal cycle was neglected by fixing the solar radiation to 413 $\mathrm{W \cdot m^{-2}}$. Finally, the initial temperature profile was defined using the time- and space-averaged temperature field over the last 10 days of a radiative–convective equilibrium simulation run in the same setting, except for the absence of rotation and a domain size that was reduced to $64 \times 64\ \mathrm{km}^2$. The resulting temperature profile was perturbed horizontally and vertically with white noise to produce heterogeneity in the initial temperature distribution.

The model was run for 100 days, during which three-dimensional (3D) outputs were saved once a day. The self-aggregation of deep convection results in the formation of a single TC within the domain as of day 18 of the simulation. In the following, this simulation will be referred to with the label "CTRL".

2.2 | Tropical cyclones in a realistic setting

The realistic simulation was conducted with the Non-hydrostatic ICosahedral Atmospheric Model (NICAM) (Tomita & Satoh, 2004) as part of the DYnamics of the Atmospheric general circulation Modeled On Non-hydrostatic Domains (DYAMOND) project for the summer phase (Stevens *et al.*, 2019b). DYAMOND summer protocol prescribes a set of global storm-resolving simulations lasting 40 days and initialized with realistic conditions extracted from the European Centre for Medium-Range Weather Forecasts (ECMWF) analysis on August 1, 2016. Several simulations employing different state-of-art models were let run freely for 40 days, and results recorded after a spin-up period of 10 days. After this time, the memory of the initial conditions is lost and each model evolves independently, as expected from nonlinear systems with chaotic behaviour (Eshel, 2006). Therefore, DYAMOND outputs do not reproduce the actual atmospheric conditions of summer 2016, but rather statistically realistic conditions, including TC size distribution, intensity, and structure, as shown in Judt *et al.* (2021).

Specifically, we analyse the three-hourly outputs from a NICAM simulation run at a 3.5-km horizontal grid spacing, with 60 vertical levels from 33.16 m up to 20 km and non-interacting oceans. Although a SAM simulation was also available in the DYAMOND protocol, we chose a different model to give more robustness to our findings, but also because NICAM was proven to produce TCs with more realistic statistical properties compared with SAM (Judt *et al.*, 2021).

In order to find TCs produced by the simulation, we first run a cyclone-tracking algorithm derived from Ragone *et al.* (2018), which identifies symmetrical, strong, and long-lasting sea-level pressure (SLP) minima.

The tracking algorithm identifies 16 cyclones in the NICAM simulation, of which seven are not considered in the subsequent analysis, because they either last for very short times (less than 1.5 days), are weak (minimum SLP above 985 hPa), or make extratropical transition or landfall during their intensification phase (i.e., the time span between cyclogenesis/detection and the time of peak intensity). The criteria on intensity and duration were taken from Stevens *et al.* (2019a), while the last one was set to discard TCs that move out of the tropical oceans during their intensification phase.

We analysed the remaining nine tracks (which were already identified in Judt *et al.*, 2021) according to the methodology described in Section 2.3. Among these, three cyclones exhibit HWC formation. In the following, we show the results relative to the cyclone that displays the HWC and its role in storm intensity most clearly. This is referred to as the "NICAM" cyclone. Results relative to the other three storms that developed an HWC, consistent with those presented here, are reported in Supporting Information: S1.7.

2.3 | Analysis methods for cyclone evolution, intensity, and prestorm conditions

The centre O of the cyclone is defined as the location of the minimum SLP at each timestep, while the intensity is defined as its value. To compute the IR, a three-day running mean filter is first applied to the intensity time series to remove short-term variability, and then the finite difference between two subsequent timesteps is used to estimate its time derivative, so as to employ the shortest increment available in our data. From the TC-centred azimuthal average of the wind speed at the first vertical level (which lies around ~ 35 m), v, we compute the radius of maximum winds $r_{\max}$ at each timestep. The area of interest for the analysis, A_{i}, is defined as a circle centred on O and with a radius $r_{\mathrm{i}} = r_{\max} + r_{\mathrm{o}}$. The value of r_{o} is chosen to have r_{i} roughly corresponding to the distance from the centre at which v has a flex point (see Figure S1 in the Supporting Information), resulting in $r_{\mathrm{o}} = 8$ km in CTRL and $r_{\mathrm{o}} = 10.5$ km in NICAM. This area includes the eye and most of the eyewall, where there is active deep convection. The azimuthally averaged vertical component of wind velocity above the boundary layer ($z = 1500$ m) reaches its peak value at a distance from the centre $r \simeq r_{\max}$ and then decreases outward, becoming less than 50% of its maximum at $r \simeq r_{\mathrm{i}}$, for each timestep.

Prestorm temperature (T_{ref}), specific humidity (q_{ref}), and virtual temperature ($T_{\mathrm{v,ref}}$) profiles, used as reference, are defined for SAM as the domain-averaged initial condition vertical profiles and for NICAM as the A_{i} averages three days prior to the storm's passage, following the cyclone displacements during its evolution. Anomalies of temperature, virtual temperature, and relative humidity are defined as the A_{i}-averaged profile departures from the reference ones and are used to highlight the presence of HWC structures (see Figure 2b).

Following Ohno and Satoh (2015), we define the tropopause as the level where normalized static stability starts increasing monotonically with height. For our simulations, this corresponds approximately to the highest level where normalized static stability exceeds 1, that is,

$$\frac{N^2}{N_0^2} > 1, \tag{1}$$

with N^2 defined as the buoyancy gradient:

$$N^2 = \frac{\partial}{\partial z}\left(g \ln \frac{\theta}{\theta_0}\right), \tag{2}$$

where g is the gravitational acceleration and where $\theta_0 = 273.15$ K and $N_0 = 10^{-2}\ \mathrm{s}^{-1}$ are two constant values.

2.4 | Analysis methods for stratospheric air intrusion

To identify the intrusion of stratospheric air into the troposphere, we use a criterion (inspired by Zhang & Chen, 2012) based on moist static energy (*MSE*), a quantity that is roughly conserved in moist adiabatic processes and is largest in the stratosphere. Boundary-layer air uprising in convective plumes cannot per se produce upper-level *MSE* values exceeding near-surface values. Moreover, Polesello *et al.* (2025) showed that, in cyclones with stratospheric intrusions, upper-level diabatic heating—in the form of radiation—plays a minor role relative to stratospheric air input in warming the upper troposphere. Therefore, we interpret tropospheric values of *MSE* larger than those occurring in the near-surface region as due to stratospheric air intrusions. Specifically, *MSE* is computed as

$$MSE = c_{\mathrm{p}} T + L_{\mathrm{v}} q + gz, \tag{3}$$

where c_{p} is the dry-air specific heat at constant pressure, L_{v} is the latent heat of vaporization, and g is the gravitational acceleration. *MSE* is averaged over A_{i} for each vertical level. We then define a critical threshold, $MSE_{\mathrm{crit}}(t)$,

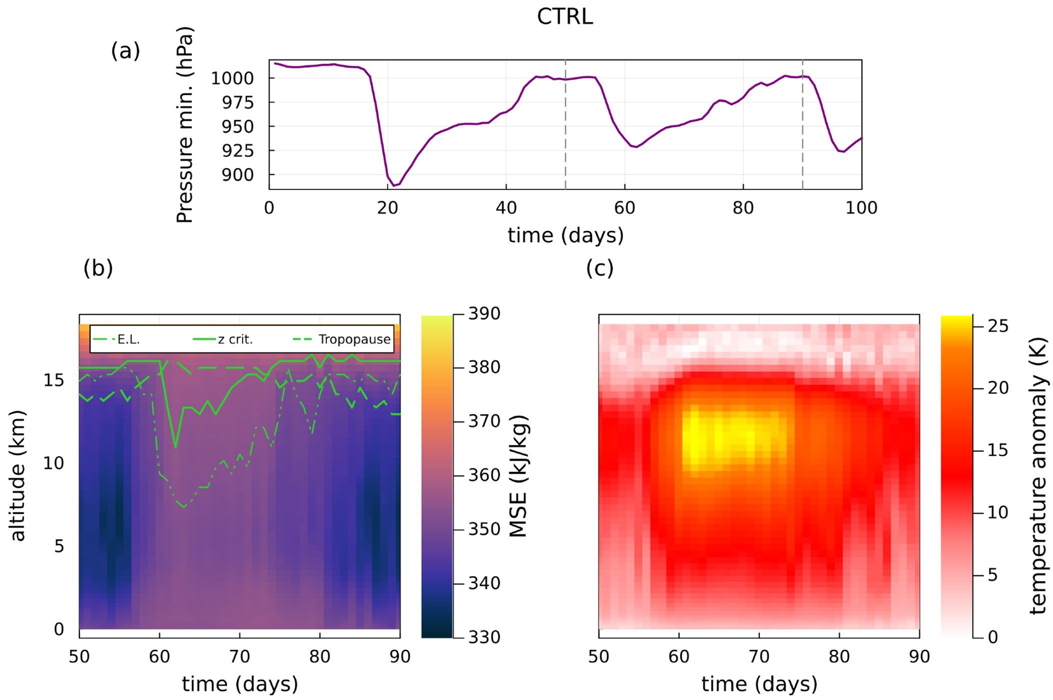

FIGURE 2 CTRL simulation: time evolution of A_i-averaged (a) *MSE* (shading), tropopause height, z_{crit} height, and *EL* height, (b) temperature anomaly with respect to T_{ref}, and (c) cyclone intensity, highlighting the timeframe analysed between the grey dashed lines. Here and in the following figures, averages are computed over A_i as described in Section 2.3. Note that the effects of sub-daily variability cannot be deducted from these plots, as CTRL instantaneous outputs are saved once per day.

above which air is assumed to have a component of stratospheric origin. This threshold is set as the maximum between an average *MSE* tropopause value (ranging from 355–360 $kJ \cdot kg^{-1}$ in the two simulation setups) and the largest A_i-averaged *MSE* value observed in the TC boundary layer between t_0 (cyclogenesis) and t. The height where $MSE(z,t) = MSE_{crit}(t)$ is defined as $z_{crit}(t)$.

The equilibrium level height (*EL*) is then computed to provide an estimate of the convection depth. To this aim, we first compute the temperature profile for an ascending air parcel from the boundary layer, starting with near-surface temperature and relative humidity and following a dry adiabatic lapse rate until saturation, then switching to a moist adiabatic profile ($T_{m.a.}$). The first vertical level above the boundary layer where virtual temperature exceeds the moist adiabatic profile ($z|T_v(z) > T_{v,\,m.a.}(z)$) is computed at each grid point, and *EL* is defined as its average over A_i. In the presence of active convection, a high *EL* is associated with deep convection, whereas a low *EL* corresponds to convection being limited to the lower troposphere due to the presence of a stable upper-air layer.

To capture the role of the HWC in the cyclone intensity, we introduce a new framework to quantify reductions in HSLP driven by the upper-level warm anomaly. Although the hydrostatic approximation does not account for the dynamic component and can thus deviate from the total pressure, we found through testing that the difference between A_i-averaged HSLP and SLP is very small (a few per cent) compared with the fluctuations of SLP during the simulations (see Figure S7 in Supporting Information S1.4). We thus compute HSLP from different temperature profiles, as obtained considering different physical processes and mechanisms. To this aim, we decompose the virtual temperature profiles as

$$T_v(z,t) = T_{v,\,m.a.}(z,t) + \Delta T_{v,\,low}(z,t) + \Delta T_{v,\,up}(z,t), \quad (4)$$

where the subscript "m.a." refers to the moist adiabatic profile obtained by lifting a near-surface air parcel adiabatically (following the dry or the moist lapse rate, depending on its relative humidity) up to the level where its temperature becomes lower than $T_{v,ref}$, and using the prestorm profile above that level (see Figure S2 in the Supporting Information). In other words, $T_{v,\,m.a.}$ represents the warmest temperature profile that could be obtained in response to the diabatic fluxes at the air–sea interface and considering only adiabatic processes within the troposphere. In Equation (4):

1. $T_{v,\,m.a.}(z,t)$ is the moist adiabatic profile at time t;
2. $\Delta T_{v,\,low}(z,t)$ is the difference between the model output virtual temperature $T_v(z,t)$ and $T_{v,\,m.a.}(z,t)$ below $z_{crit}(t)$; and

3. $\Delta T_{\mathrm{v,\,up}}(z,t)$ is the same as point 2, but evaluated above $z_{\mathrm{crit}}(t)$ and up to the model's vertical limit.

This decomposition allows us to add two more temperature profiles along the moist adiabatic and the model output: $T_{\mathrm{v,\,m.a.}}(z,t)+\Delta T_{\mathrm{v,\,low}}(z,t)$, which corresponds to the actual temperature profile below z_{crit}, which can be colder than the moist adiabat in the presence of CAPE, and $T_{\mathrm{v,\,m.a.}}(z,t)+\Delta T_{\mathrm{v,\,high}}(t)$, which, when z_{crit} is below the tropopause height, accounts for the upper-level warm core, where virtual temperature is higher than the value that could be obtained by lifting the boundary-layer air adiabatically with the largest entropy it ever attained (see Figure S3 in the Supporting Information for a visual example).

HSLP values are then computed using all these different profiles. By comparing HSLP derived from the actual model profile with that from $T_{\mathrm{v,\,m.a.}}+\Delta T_{\mathrm{v,\,low}}(t)$, we get a conservative estimate of the HWC contribution to TC intensity: the difference between the two pressures is due to the upper-level warming associated with the intrusion of stratospheric air into the troposphere.

3 | TIME EVOLUTION OF TC INTENSITY

3.1 | Idealized simulation

The CTRL simulation produced a single TC showing an oscillatory behaviour of its intensity. This oscillation corresponds to the formation of the TC, followed by its complete dissipation and its subsequent re-intensification (Figure 2c), as discussed in detail in Polesello *et al.* (2025). The physical processes at the root of the oscillation, which are not the main focus of this work, are discussed in Appendix A, where a simplified model of TC intensity and air-column static stability evolution is introduced. Here we focus on the time interval 50–90 days, corresponding to the second life-cycle window of the cyclone, as defined by Polesello *et al.* (2025). This interval was chosen, as it shows more clearly the effects of the HWC on HSLP and IR. Results relative to the complete run are reported in Supporting Information: S1.6 (and Figures S11–S13). The evolution of the cyclone displays an intensification phase, up to day 62 when the TC reaches its peak intensity, corresponding to a minimum SLP of $\sim$ 930 hPa, followed by a slower decay until day 90 (Figures 2a). As the cyclone develops, the troposphere warms up, leading to positive temperature anomalies of more than 25 K centred at a height of about 10–12 km (Figure 2b,c).

The *MSE* in the upper troposphere reaches values larger than MSE_{crit} (Figure 2b), indicating that boundary-layer air in adiabatic ascent cannot be solely responsible for these upper-level properties. It was shown in Polesello *et al.* (2025) that diabatic warming by interactive radiation was not necessary to generate the anomaly, leading to the conclusion that stratospheric air was involved in the generation of the HWC. Consistently, the height z_{crit}, which initially lies above the tropopause, quickly drops below it during the intensification phase, indicating the subsidence of stratospheric air at least down to an altitude of approximately 10 km. Eventually, z_{crit} recovers slowly to prestorm conditions during the weakening phase of the cyclone. The cooling during this phase is likely due to lateral advection of colder air or rain evaporation, as the role of radiation was shown to be marginal by Polesello *et al.* (2025). The cooling contributes to the dissipation of the warm anomaly and to the build-up of CAPE (Polesello *et al.*, 2025), leading to repetition of the cycle, with a new cyclone that forms and decays.

The equilibrium level loosely follows the same time evolution, with the addition of small fluctuations associated with changes in the boundary-layer *MSE*: in prestorm conditions, the *EL* is at about 15 km, then the buoyancy increase of the upper-level air lowers it rapidly to about 7 km, after which a slow recovery phase occurs (Figure 2b).

The vertical temperature profiles (Figure 3) provide additional insight into the cyclone intensification process. During the intensification phase, the tropospheric temperature approaches the moist adiabatic profile (Figure 3a), while the descent of stratospheric air eventually raises temperatures beyond the moist adiabatic lapse rate above z_{crit} (Figure 3b), thereby stabilizing the atmospheric column. During the dissipation stage (i.e., from the time of peak intensity to the end of detection), the continuing decrease of z_{crit} is associated with a larger portion of the column having a temperature warmer than the one associated with the moist adiabatic ascent of boundary-layer air, inhibiting convection further and eventually leading to cyclone dissipation. Throughout this phase, no evidence of concentric eyewall replacement was found (see Figure S4 in Supporting Information: S1.2), ruling out the possibility that it might have played a relevant role in setting the dissipation.

The HSLP time series in Figure 4 reveal that the minimum HSLP derived from the actual temperature profile, p_{env}, at the cyclone peak intensity (i.e., when the HSLP is at its minimum, at day 62) is about 10 hPa lower than that obtained from the moist adiabatic profile, $p_{\mathrm{m.a.}}$. This indicates that the presence of a high-level warm core can (slightly) lower the system minimum HSLP, thus strengthening the peak intensity achieved by the cyclone.

However, around the time when z_{crit} becomes lower than the tropopause, marking the intrusion of

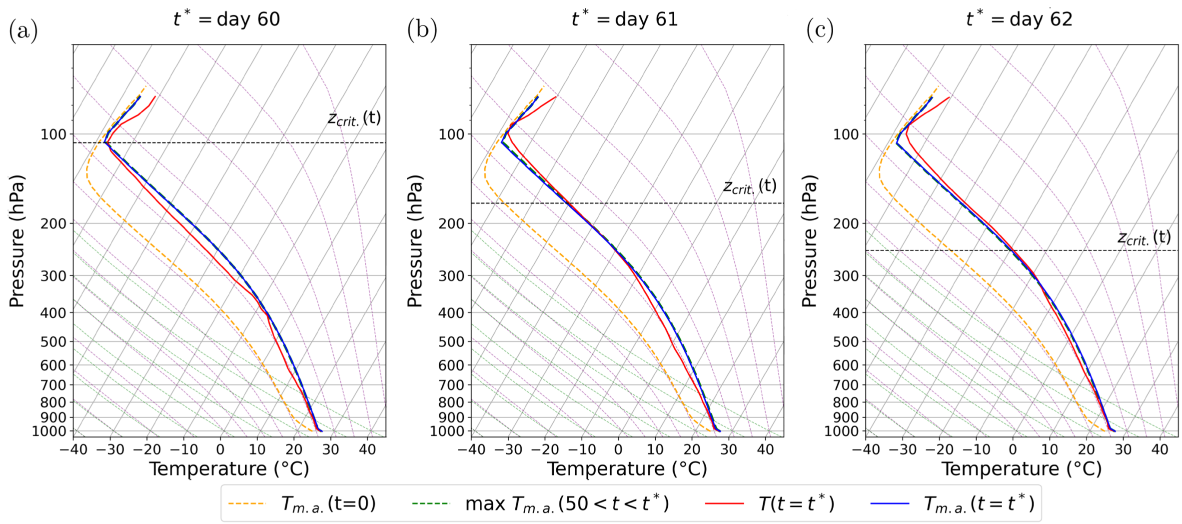

FIGURE 3 CTRL simulation: A_i-averaged absolute temperature profiles (red solid line), the moist adiabat at time t^* indicated in the title of each panel (blue solid line), the prestorm moist adiabat (orange dashed line), and the warmest moist adiabat prior to t^* (green dashed line). The horizontal black line indicates z_{crit} at t^* in pressure coordinates. The three panels refer to the three times t^* highlighted in Figure 4: (a) $t^* = 60$ days in the intensification phase, (b) $t^* = 61$ days, with the beginning of the stratospheric air intrusion, and (c) $t^* = 62$ days, at the SLP minimum.

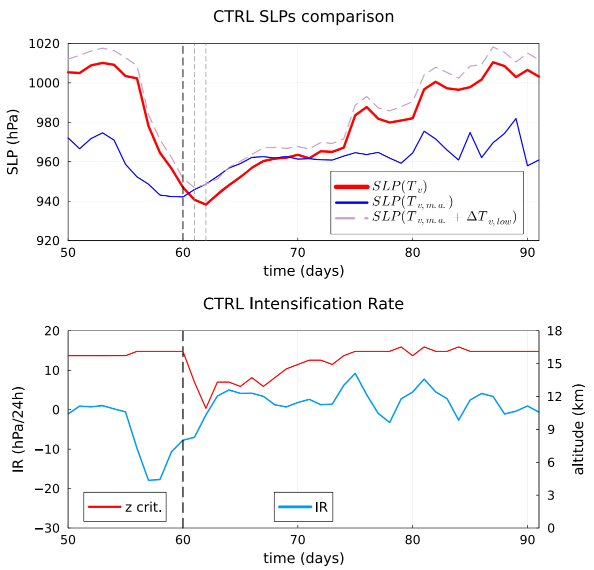

FIGURE 4 CTRL simulation. Upper panel: A_i-averaged HSLP evolution computed using the different instantaneous temperature profiles, as indicated in the inset. The black vertical dashed line indicates the last time at which z_{crit} is above the tropopause. Grey vertical lines and the black line highlight the timesteps represented in Figure 3. Lower panel: IR evolution computed as per Section 2.3, highlighting the same timestep as in the upper panel plot.

stratospheric air in the troposphere, the IR starts decreasing (Figure 4). Eventually, the IR reaches negative values, marking the cyclone dissipation. The decrease in IR is attributed to the role of upper-level warming in stabilizing the air column.

3.2 | Realistic simulation

The NICAM cyclone investigated in this section moves in the northern Atlantic basin, starting on August 16. Initially, it follows a mainly westward trajectory, until it reaches its peak intensity of ~ 915 hPa (Figure 5c) close to the Bahamas, after eight days of intensification. In the later stage it moves northward, approaching the USA coastline while losing intensity.

Similarly to the idealized CTRL case, this cyclone exhibits a warm-core temperature anomaly in the upper troposphere, at altitudes between 11 and 15 km, that peaks at +15 K around the time of maximum intensity (Figure 5b,c). The *MSE* in the upper troposphere becomes larger than MSE_{crit} (Figure 5b), suggesting the intrusion of air of stratospheric origin. The interpretation is supported further by an isentropic analysis inspired by that of Dauhut *et al.* (2017), which shows downward transport of large *MSE* air at the tropopause height (see Figure S6 in Supporting Information: S1.3). During the intensification period, the temperature profile in the upper troposphere rises above the adiabatic profile (Figure 6). The consequent formation of a HWC leads to a reduction of HSLP below the values obtained from the moist adiabatic profiles during August 22 at 0300 UTC. Indeed, the minimum HSLP for the moist adiabatic case is about 960 hPa, while it drops to 940 hPa for the actual temperature profile, indicating a 20-hPa deepening of the depression associated with the upper-level warm core (Figure 7).

The stratospheric intrusion, marked by z_{crit} decreasing below the tropopause, appears close to the time when the

Quarterly Journal of the Royal Meteorological Society RMetS

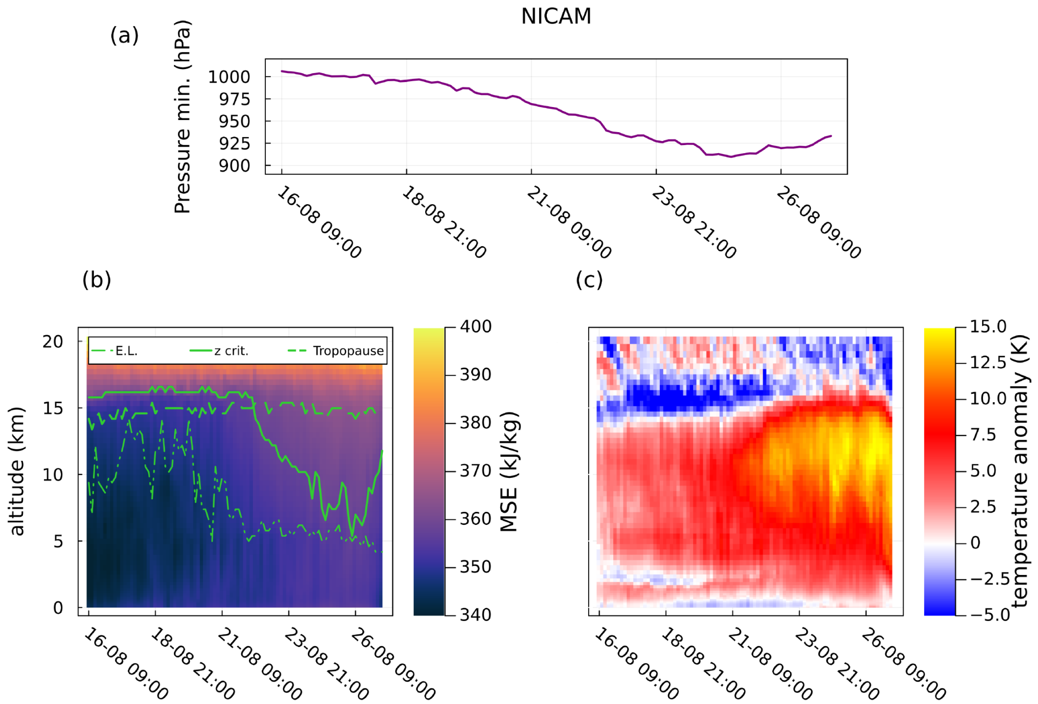

FIGURE 5 As Figure 2 for NICAM.

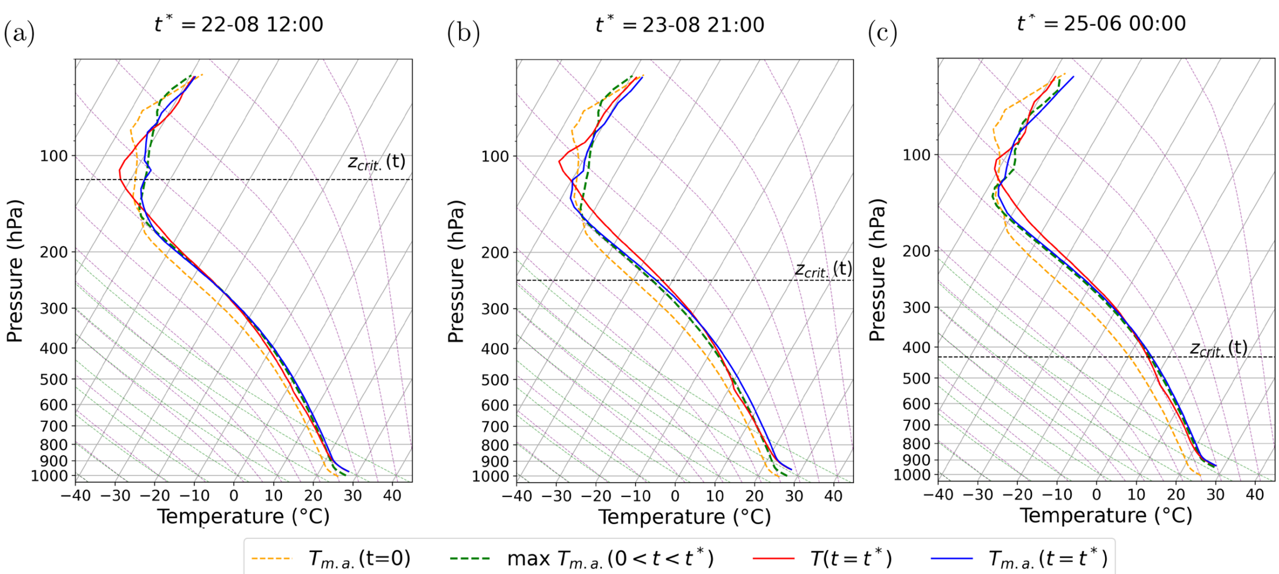

FIGURE 6 As Figure 3 for NICAM. These plots refer to the three timesteps highlighted in Figure 7 by the vertical grey and black lines: (a) beginning of stratospheric air intrusion in the troposphere, (b) intensification with lowering z_{crit}, and (c) minimum SLP.

IR begins to decrease (Figure 7), suggesting that the intensity tendency might be affected by the upper-level warm anomaly as discussed previously. Similarly to SAM, the decrease in IR is not caused by an eyewall replacement cycle, which instead occurs about four days later, when the IR becomes negative (see Figure S5 in Supporting Information: S1.2), thus ruling out this process as the initial cause of the intensification decay.

A closer look at Figure 6b shows that, during the intensification phase, the height at which the environmental temperature becomes warmer than the moist adiabat (around 400 hPa) lies significantly below z_{crit}. This behaviour can be explained by two factors. First, we note that stratospheric air is much drier than that in the troposphere. Therefore, while mixing with the intruding air might increase the eyewall's temperature, its *MSE* might

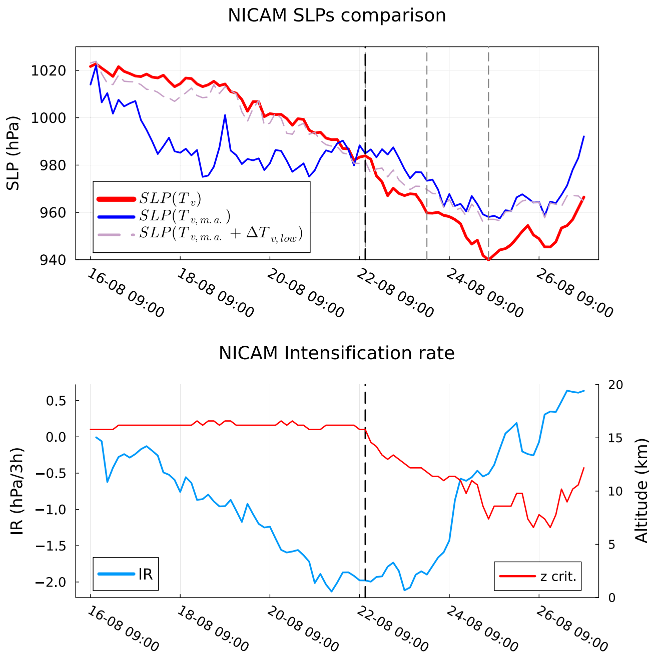

FIGURE 7 As Figure 4 for NICAM.

be negatively affected by the reduction in moisture, thus increasing z_{crit} in those regions. Second, the choice of MSE_{crit} as the maximum MSE in the boundary layer leads to z_{crit} being an upper limit for the base of the stratospheric intrusion, which could actually reach lower levels when stratospheric air has lower MSE than boundary-layer air. For this reason, we stress that the HWC contribution to HSLP obtained in our analysis is a lower limit and the effective contribution might be larger.

A similar behaviour to that presented in this section is obtained for the three other NICAM cyclones, as shown in Supporting Information: S1.7 with Figures S14–S22. This allows us to confirm that, in the realistic simulation, the signatures of the HWC effects on TC evolution are consistent with the mechanisms identified in the idealized simulation, namely the following.

- The stratospheric air layer delimited by z_{crit} can intrude into the upper troposphere, resulting in the formation of a HWC.
- The HWC initially contributes to intensifying the cyclone by reducing the minimum HSLP beyond what could be achieved if the cyclone were driven solely by moist convection.
- At the same time, the HWC stabilizes the atmospheric column by warming the air beyond the moist adiabatic lapse rate, as demonstrated by the reduction in EL (Figure 5a). This can limit the depth of convective motion and reduce the IR (Figure 7).

However, in this realistic case, additional effects from, for example, the heterogeneity of the surface boundary conditions or the presence of other disturbances (such a varying vertical wind shear) cannot be ruled out as principal drivers of the weakening of the cyclone.

4 | CONCLUSIONS

In this work, we investigate the role of HWCs in TC evolution using high-resolution numerical simulations. We analyse an idealized simulation performed with the SAM atmospheric model in rotating radiative–convective equilibrium on a doubly periodic domain and a realistic simulation performed with the NICAM global model as part of the DYAMOND summer project.

Our results show that air of stratospheric origin intrudes into the upper troposphere, contributing to HWC development. The level z_{crit} provides a conservative estimate of the base of the stratospheric intrusion and extends into the mid-troposphere, consistent with observational evidence (Grant *et al.*, 2008). We find that the HWC plays a dual role in TC evolution. As reported in previous studies, HWCs enhance cyclone intensity by reducing the HSLP through warming (Kieu *et al.*, 2016; Ohno & Satoh, 2015; Zhang & Chen, 2012). At the same time, however, they stabilize the atmospheric column (Rodgers *et al.*, 1990), suppressing convection and ultimately contributing to cyclone weakening. These dual roles of the HWC are not contradictory; rather, they operate on different time-scales. The reduction in HSLP, which depends directly on air density through its temperature, acts on the time-scale of stratospheric subsidence. Conversely, the stabilization and dissipation driven by the HWC act on a longer time-scale, as they face the inertia of the cyclone and likely go through a direct effect on convective activity, which precedes intensity changes (Rodgers *et al.*, 1990). Those results are robust to reasonable variations in the definition of z_{crit}. In fact, we conducted sensitivity tests on z_{crit} height, demonstrating that the decrease in HSLP due to HWC formation is nearly unaltered even for variations in z_{crit} of the order of 1500 m. It is worth stressing that our definition of z_{crit} is an upper limit to the height at which stratospheric intrusions affect the troposphere. Indeed, dilution of boundary-layer MSE due to entraining convective plumes results in an overestimation, based on our methodology, of the maximum upper-level MSE that can be attained directly through convection. Considering that the aim of this work is to identify the occurrence of stratospheric intrusions and assess their effects, the use of conservative metrics is well suited for documenting their impact on TC evolution, which can be even larger than what is shown.

In the CTRL simulation, where other TC damping processes are absent (constant SST and weak vertical wind shear), the HWC emerges as the dominant dissipation mechanism. In the NICAM simulation, cyclone evolution is influenced by multiple competing processes, making it harder to isolate individual contributions. Nonetheless, the characteristics and timing of the upper tropospheric warming in relation to the changes in the IR—similar to what is observed in CTRL—suggest that the HWC can also play a critical role in the dissipation of realistic cyclones.

Overall, the consistency of the results across the different settings and models increases confidence in their robustness. However, both simulations share the absence of interactive oceans, which, if included, might dampen latent heat fluxes from the sea surface, as TC-induced ocean mixing reduces the SST.

The framework used in this study requires some methodological considerations. Our analysis is carried out over a cylindrical region surrounding the cyclone centre, including both the eye and eyewall. While it is well known that the upward motion occurs on slanted surfaces of constant angular momentum, Polesello *et al.* (2025) showed that a more complex analysis following angular momentum surfaces does not change the results significantly. Moreover, the assumption of adiabatic ascent is certainly invalid in the eye, where subsidence occurs. However, since the circular area that defines the cylinder is much larger than the eye, it is mainly representative of the eyewall region. On the other hand, excluding the eye would also neglect the region of strongest stratospheric subsidence (Kieu *et al.*, 2016).

Thus, while our approach provides only an approximate and conservative quantification of the HSLP anomaly, we argue that it is sufficient to capture the role of the HWC and to identify mechanisms influencing TC intensity. Regarding the azimuthal averaging, we acknowledge that this implicitly assumes an axisymmetric HWC structure. This assumption is well justified for SAM, where environmental wind shear is absent, but less so for the more realistic NICAM simulation. While in the latter simulation a certain degree of asymmetry is indeed visible from spatial distributions of wind speed, *MSE*, z_{crit}, and so on (not shown), the *MSE* anomaly (and, thus, the regions where z_{crit} is low) remains concentrated within A_{i}, suggesting that azimuthal averaging does not dilute the signal substantially in this case. We also note that any residual dilution would reinforce the conservative nature of our HSLP estimate further.

It is important to note that our analysis has been performed on a limited number of cyclones. In the 30-day long realistic NICAM simulation, four out of nine cyclones analysed develop HWCs. The detection of even only one cyclone showing evidence of stratospheric intrusion and its effect on TC evolution demonstrates the relevance of the processes that we describe. It remains to be understood why some cyclones form HWCs while others do not. Among the NICAM cyclones, those that eventually develop an HWC exhibit higher boundary-layer *MSE* at the time of their detection/cyclogenesis, suggesting that stronger initial convection may facilitate stratospheric interaction through more frequent overshoots beyond the tropopause. We also observed that inertial stability plays a role in the development of the HWC. This supports the idea that a positive feedback loop may arise initially, where increasing inertial stability confines subsidence warming in a small inner-core area, favouring intensification and increasing inertial stability further (Schubert & Hack, 1982), until increasing static stability becomes the dominant factor and limits updrafts. Further investigation, over larger datasets, would be needed to verify these hypotheses.

The insights gained from this study highlight the importance of an accurate representation of the stratosphere (and its circulation) in numerical models of TC evolution. Our results demonstrate that stratospheric intrusions play a non-negligible role in the TC life cycle, influencing both intensification and dissipation phases. While, to the best of our knowledge, no study has demonstrated directly that improving the representation of the stratosphere in numerical models leads to more reliable TC intensity forecasts, understanding the effects of stratospheric air intrusion may nonetheless contribute to constraining key metrics relevant to PI better, such as the outflow level temperature (Gilford *et al.*, 2017).

ACKNOWLEDGMENTS

The authors thank Tom Beucler, Hamish Ramsay, and two anonymous reviewers for insightful comments and constructive feedback on earlier versions of this work.

This work is partially funded by the National Recovery and Resilience Plan project TeRABIT (Terabit network for Research and Academic Big data in Italy—IR0000022—PNRRMissione4—Componente2—Investimento3.1—CUPI53C21000370006) in the frame of the European Union—NextGenerationEU funding. C. Muller gratefully acknowledges funding from the European Research Council (ERC) under the European Union's Horizon 2020 research and innovation program (Project CLUSTER, Grant 805041). This work is an outcome of the project MIUR—Dipartimenti di Eccellenza 2023–2027.

This work used resources of the Deutsches Klimarechenzentrum (DKRZ) granted by its Scientific Steering Committee (WLA) under project bb1153. Open access publishing facilitated by Universita degli Studi di Milano-Bicocca, as part of the Wiley - CRUI-CARE agreement.

DATA AVAILABILITY STATEMENT

The data that support the findings of this study are available from the corresponding author upon reasonable request.

ORCID

Andrea Davin https://orcid.org/0009-0009-8256-3803
Caroline Muller https://orcid.org/0000-0001-5836-5350

REFERENCES

Bister, M. & Emanuel, K.A. (1998) Dissipative heating and hurricane intensity. *Meteorology and Atmospheric Physics*, 65, 233–240.

Bister, M. & Emanuel, K.A. (2002) Low frequency variability of tropical cyclone potential intensity 1. Interannual to irtterdecadal variability. *Journal of Geophysical Research: Atmospheres*, 107, ACL 26–1–ACL 26–15.

Cangialosi, J.P., Blake, E., DeMaria, M., Penny, A., Latto, A., Rappaport, E. et al. (2020) Recent progress in tropical cyclone intensity forecasting at the national hurricane center. *Weather and Forecasting*, 35, 1913–1922.

Chacko, N. (2023) On the rapid weakening of super-cyclone amphan over the bay of bengal. *Ocean Dynamics*, 73, 359–372.

Chen, H. & Zhang, D.-L. (2013) On the rapid intensification of hurricane wilma (2005). Part ii: convective bursts and the upper-level warm core. *Journal of the Atmospheric Sciences*, 70, 146–162.

Dauhut, T., Chaboureau, J.-P., Mascart, P. & Pauluis, O. (2017) The atmospheric overturning induced by hector the convector. *Journal of the Atmospheric Sciences*, 74(10), 3271–3284.

Emanuel, K.A. (1995) Sensitivity of tropical cyclones to surface exchange coefficients and a revised steady-state model incorporating eye dynamics. *Journal of the Atmospheric Sciences*, 52, 3969–3976.

Emanuel, K.A. (1997) Some aspects of hurricane inner-core dynamics and energetics. *Journal of the Atmospheric Sciences*, 54(8), 1014–1026.

Emanuel, K. (2000) A statistical analysis of tropical cyclone intensity. *Monthly Weather Review*, 128, 1139–1152.

Emanuel, K. (2003) Tropical cyclones. *Annual Review of Earth and Planetary Sciences*, 31, 75–104.

Eshel, G. (2006) Empirically evaluating divergence rates of atmospheric trajectories. *Journal of the Atmospheric Sciences*, 63(2), 741–753.

Garner, S. (2015) The relationship between hurricane potential intensity and cape. *Journal of the Atmospheric Sciences*, 72, 141–163.

Gilford, D.M., Solomon, S. & Emanuel, K.A. (2017) On the seasonal cycles of tropical cyclone potential intensity. *Journal of Climate*, 30(16), 6085–6096.

Grant, D.D., Fuentes, J.D., DeLonge, M.S., Chan, S., Joseph, E., Kucera, P. et al. (2008) Ozone transport by mesoscale convective storms in western Senegal. *Atmospheric Environment*, 42(30), 7104–7114.

Judt, F., Klocke, D., Rios-Berrios, R., Vanniere, B., Ziemen, F., Auger, L. et al. (2021) Tropical cyclones in global storm-resolving models. *Journal of the Meteorological Society of Japan*, 99, 579–602.

Kaplan, J. & DeMaria, M. (2003) Large-scale characteristics of rapidly intensifying tropical cyclones in the north atlantic basin. *Weather and Forecasting*, 18, 1093–1108.

Khairoutdinov, M.F. & Randall, D.A. (2003) Cloud resolving modeling of the arm summer 1997 iop: model formulation, results, uncertainties, and sensitivities. *Journal of the Atmospheric Sciences*, 60, 607–625.

Kieu, C., Tallapragada, V., Zhang, D.L. & Moon, Z. (2016) On the development of double warm-core structures in intense tropical cyclones. *Journal of the Atmospheric Sciences*, 73, 4487–4506.

Kossin, J.P. & Sitkowski, M. (2012) Predicting hurricane intensity and structure changes associated with eyewall replacement cycles. *Weather and Forecasting*, 27(2), 484–488.

Kuo, H.-C., Cheng, W.-Y., Yang, Y.-T., Hendricks, E.A. & Peng, M.S. (2016) Deep convection in elliptical and polygonal eyewalls of tropical cyclones. *Journal of Geophysical Research: Atmospheres*, 121(24), 14–456.

Lavender, S.L., Hoeke, R.K. & Abbs, D.J. (2018) The influence of sea surface temperature on the intensity and associated storm surge of tropical cyclone yasi: a sensitivity study. *Natural Hazards and Earth System Sciences*, 18, 795–805.

Lin, I.I., Goni, G.J., Knaff, J.A., Forbes, C. & Ali, M.M. (2013) Ocean heat content for tropical cyclone intensity forecasting and its impact on storm surge. *Natural Hazards*, 66, 1481–1500.

Mei, W., Pasquero, C. & Primeau, F. (2012) The effect of translation speed upon the intensity of tropical cyclones over the tropical ocean. *Geophysical Research Letters*, 39, 7.

Moon, Z. & Kieu, C. (2017) Impacts of the lower stratosphere on the development of intense tropical cyclones. *Atmosphere*, 8, 128.

Muller, C. & Romps, D. (2018) Acceleration of tropical cyclogenesis by self-aggregation feedbacks. *Proceedings of the National Academy of Sciences of the United States of America*, 115(12), 2930–2935.

Ohno, T. & Satoh, M. (2015) On the warm core of a tropical cyclone formed near the tropopause. *Journal of the Atmospheric Sciences*, 72, 551–571.

Ooyama, K. (1969) Numerical simulation of the life cycle of tropical cyclones. *Journal of the Atmospheric Sciences*, 26, 3–40.

Polesello, A., Charinti, G.A., Meroni, A.N., Muller, C.J. & Pasquero, C. (2025) Intensity oscillations of tropical cyclones: surface versus mid and upper tropospheric processes. *Journal of Advances in Modeling Earth Systems*, 17, e2024MS004613.

Ragone, F., Mariotti, M., Parodi, A., von Hardenberg, J. & Pasquero, C. (2018) A climatological study of western mediterranean medicanes in numerical simulations with explicit and parameterized convection. *Atmosphere*, 9, 397.

Rodgers, E.B., Stout, J., Steranka, J. & Chang, S. (1990) Tropical cyclone-upper atmospheric interaction as inferred from satellite total ozone observations. *Journal of Applied Meteorology and Climatology*, 29(9), 934–954.

Rotunno, R. & Emanuel, K.A. (1987) An airsea interaction theory for tropical cyclones. Part ii: evolutionary study using a nonhydrostatic axisymmetric numerical model. *Journal of the Atmospheric Sciences*, 44, 542–561.

Rousseau-Rizzi, R. & Emanuel, K. (2019) An evaluation of hurricane superintensity in axisymmetric numerical models. *Journal of the Atmospheric Sciences*, 76, 1697–1708.

Schade, L.R. & Emanuel, K.A. (1999) The oceans effect on the intensity of tropical cyclones: results from a simple coupled

atmosphereocean model. *Journal of the Atmospheric Sciences*, 56, 642–651.
Schubert, W.H. & Hack, J.J. (1982) Inertial stability and tropical cyclone development. *Journal of Atmospheric Sciences*, 39(8), 1687–1697.
Smith, R.K., Kilroy, G. & Montgomery, M.T. (2021) Tropical cyclone life cycle in a threedimensional numerical simulation. *Quarterly Journal of the Royal Meteorological Society*, 147, 3373–3393.
Stevens, B., Satoh, M., Auger, L., Biercamp, J., Bretherton, C.S., Chen, X. et al. (2019a) Dyamond: the dynamics of the atmospheric general circulation modeled on non-hydrostatic domains.
Stevens, B., Satoh, M., Auger, L., Biercamp, J., Bretherton, C.S., Chen, X. et al. (2019b) Dyamond: the dynamics of the atmospheric general circulation modeled on non-hydrostatic domains. *Progress in Earth and Planetary Science*, 6, 61.
Tomita, H. & Satoh, M. (2004) A new dynamical framework of nonhydrostatic global model using the icosahedral grid. *Fluid Dynamics Research*, 34(6), 357–400.
Wang, H. & Wang, Y. (2014) A numerical study of typhoon megi (2010). Part i: rapid intensification. *Monthly Weather Review*, 142(1), 29–48.
Wing, A.A., Camargo, S.J. & Sobel, A.H. (2016) Role of radiativeconvective feedbacks in spontaneous tropical cyclogenesis in idealized numerical simulations. *Journal of the Atmospheric Sciences*, 73, 2633–2642.
Xu, J. & Wang, Y. (2018) Dependence of tropical cyclone intensification rate on sea surface temperature, storm intensity, and size in the western north pacific. *Weather and Forecasting*, 33, 523–537.
Zhang, D.L. & Chen, H. (2012) Importance of the upper-level warm core in the rapid intensification of a tropical cyclone. *Geophysical Research Letters*, 39, L02806.

SUPPORTING INFORMATION

Additional supporting information can be found online in the Supporting Information section at the end of this article.

How to cite this article: Davin, A., Charinti, G.A., Muller, C., Polesello, A. & Pasquero, C. (2026) Stratospheric influence on tropical cyclone evolution. *Quarterly Journal of the Royal Meteorological Society*, e70280. Available from: https://doi.org/10.1002/qj.70280

APPENDIX A. MINIMAL MODEL OF TC OSCILLATIONS

We derive here a simple physically based model that reproduces the oscillatory behaviour observed in the CTRL simulation described above. To this end, in this section we build a low-order system of ordinary differential equations (ODEs) to model the troposphere–stratosphere interaction and its effects on TC intensity, excluding other mechanisms that are known to affect TC strength such as SST variations and vertical wind shear. This minimal model is designed to isolate the essential feedbacks leading to an oscillatory behaviour, rather than to reproduce realistic IRs. As such, it should be interpreted as a conceptual tool to identify the interplay between intensification and static stability. To keep the model as simple as possible while including the key physical processes, we use two prognostic, adimensional variables: intensity of the cyclone (v) and static stability of the troposphere (s). Other relevant quantities are expressed as functions of these variables. The ODE system is defined as

$$\frac{ds}{dt} = \alpha\Theta(v - v_c) - \gamma s, \tag{A1}$$

$$\frac{dv}{dt} = \frac{av}{1+s}\Theta(v - bs) - dv^2, \tag{A2}$$

where Θ denotes the Heaviside function.

In this formulation, $s = 0$ corresponds to marginal stability, that is, a moist adiabatic temperature profile, while positive values indicate increased stability. Equation (A1) describes the relaxation of the tropical atmosphere towards marginal stability on a time-scale γ^{-1}. When the cyclone is sufficiently strong ($v > v_c$), interaction with the stratosphere warms the upper troposphere, which increases static stability, as represented by the first term on the right-hand side of Equation (A1). Cyclone intensity evolves according to Equation (A2), with two competing terms: an energy source term from surface fluxes and a frictional dissipation term. Dissipation is proportional to wind speed squared, $-dv^2$, with d setting its strength. The source term was conceived to mimic the WISHE effect, in which there is a positive feedback between wind intensity and surface enthalpy fluxes (Emanuel, 1995). For this reason, the intensity source term is a function of wind speed and is modelled as av. However, this surface energy flux contributes to the strengthening of the cyclone only if (a) an energy barrier layer above the boundary layer is overcome and (b) vertical updrafts in the cyclone reach the tropopause, releasing the latent heat the air contains through the condensation of water vapour. For the first point, we assume that in the presence of a strong barrier layer, with inhibiting energy considered to be proportional to static stability, bs, vertical motion is not initiated and the cyclone does not intensify. The cyclone can intensify when the energy of the lower near-surface layer (considered to be proportional to v) overcomes the energy of the barrier layer, $v > bs$. Clearly, when $s = 0$ there is no barrier layer and a small wind perturbation can develop into an intense cyclone. For the second point above, we consider that the surface energy flux contributes to the time evolution of the cyclone only in the fraction that gets released in the air column: assuming that a larger stability lowers the equilibrium level below the tropopause where temperatures are higher, updrafts release only a fraction of the energy they contain, modelled as $1/(1+s)$. Thus, when $s=0$ (marginal stability conditions), all the energy input at the sea surface (av) leads to the strengthening of the cyclone, while for stable stratification, $s>0$, only part of it ($av/(1+s)$) contributes to the intensification, and only if the barrier layer is overcome. To avoid singularities in the system of equations, we substitute the Heaviside step function $\Theta(x)$ with a smoothed version of it:

$$\Theta(x) = \left(\frac{2}{\pi}\arctan(x) + 1\right)/2. \tag{A3}$$

Figure A1 shows the time evolution of the two variables starting from the initial conditions $s(0)=1$ and $v(0)=0$, for the following list of adimensional parameters, which will be referred to as "base" settings: $a=5, b=5, d=0.03$, $\alpha=0.4$, $\gamma=0.06$, $v_c=10$. The time evolution of the two variables indicates that the system shifts rapidly towards a limit cycle.

Rather than exploring the parameter space fully (results are partly presented in Supporting Information: S1.5, with a bifurcation diagram presented in Figure S8 and the results of a sensitivity test in Figures S9 and S10), here we focus on the physical processes underlying the oscillations, noting simply that the oscillatory behaviour is robust to a reasonable change of parameter values. Starting from a very weak cyclone, the intensity increases slowly, up to a point (time t_A in Figure A1) at which the wind speed v becomes larger than bs and the energy-barrier layer is overcome. At this point, the WISHE mechanism is responsible for a very fast growth of the intensity of the TC. In the absence of any tropospheric–stratospheric interaction, the cyclone would reach a steady-state intensity, when the energy input equals the dissipation. This would occur for $v=a/d=167\,\mathrm{m{\cdot}s^{-1}}$ for the base parameter values. Instead, the fast-increasing speed leads quickly to an increase of the static stability of the air column, which reduces the effective energy input into the system (despite the increasing intensity, the term $av/(1+s)$ decreases). At time t_B, the energy input term equals the energy dissipation term. The still growing stability keeps reducing the energy input term to values lower than the dissipative term. This generates a (relatively slow) weakening of the cyclone, which continues until time t_C, when the rising motion stops ($v<bs$, the barrier layer inhibits further updrafts) and the intensity of the cyclone decreases abruptly. At time t_D, the cyclone becomes so weak that the stratosphere–troposphere interaction is interrupted and the upper-level warm anomaly starts decreasing (s decreases), allowing for a very slow recovery of the wind speed. When the stability parameter s becomes small enough, deep convection is activated again, $v>bs$) and the cyclone intensifies rapidly again, repeating the whole cycle.

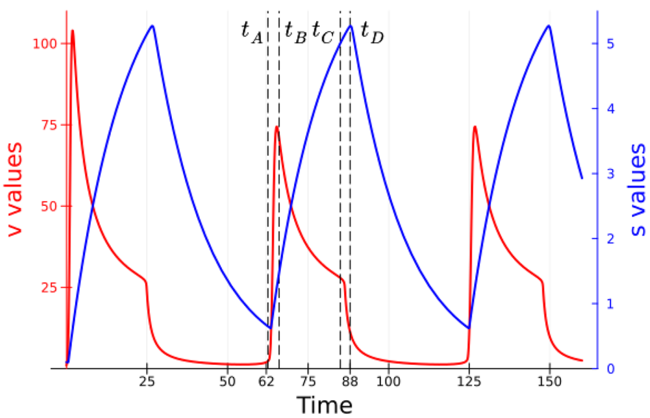

FIGURE A1 Time evolution of the adimensional variables representing cyclone intensity (v) and static stability (s) in the simple ODE model for the base parameter set. Vertical dashed lines highlight the timesteps discussed in Appendix A.

The oscillatory behaviour found in the base parameter setting is in agreement with the results of the CTRL simulation, where the idealized settings produced three consecutive intensification phases. In more realistic settings, a limit cycle is not expected. Real TCs dissipate for factors that are not included in the idealized doubly periodic setting described in the previous section, nor in the model presented above. Those factors include a vertical wind shear, extratropical transitions, colder SSTs, and landfalls. These processes shorten the storm's life cycle and create a more hostile environment to cyclone intensification, preventing the emergence of oscillatory behaviour. Their exclusion likely favours the emergence and persistence of the oscillatory behaviour identified by the model. Furthermore, the simplified WISHE-like parameterization adopted here does not represent boundary-layer thermodynamics or realistic SST feedbacks explicitly, and should therefore be interpreted only as a conceptual representation of enthalpy input. Consequently, the model is not intended to provide a quantitatively realistic description of TC evolution, but rather to isolate and clarify a possible physical mechanism through which HWC formation and the associated increase in static stability may modulate cyclone intensity under idealized conditions. Despite these limitations, this simple model remains a useful conceptual tool for visualizing a mechanism that may still operate in more realistic environments.